JOM, Vol. 72, No. 2, 2020
https://doi.org/10.1007/s11837-019-03954-2

Liquid-Metal-Mediated Recrystallization of Zinc Under Ambient Conditions

J.E. NORKETT [1,2,3] and V.M. MILLER[2]

1.—Department of Materials Science and Engineering, North Carolina State University, Raleigh, NC 27695, USA. 2.—Department of Materials Science and Engineering, University of Florida, Gainesville, FL 32611, USA. 3.—e-mail: jnorkett@ufl.edu

Liquid-metal-mediated recrystallization is a poorly understood facet of liquid metal embrittlement that has never before been the subject of systematic study. In this work, commercially pure Zn sheet with varied grain size and amount of prior deformation is exposed to liquid eutectic Ga-In, and the resulting microstructural evolution is characterized. The penetration rate of the liquid into the grain boundary network is observed to be strongly dependent on grain size, with little or no dependence on prior deformation. However, the extent of recrystallization and the accompanying evolution of crystallographic and morphologic texture is strongly dependent on prior deformation.

INTRODUCTION

Liquid metal bearing circuits are an enabling technology for a wide range of applications, including flexible thermoelectrics,[1] reconfigurable antennas,[2–5] and stretchable devices.[6–9] However, the implementation of liquid metal circuit technology is inhibited by the possibility of liquid metal embrittlement (LME) at the electrical contacts or after damage to the circuits releases the liquid.

When liquid and solid metals are in physical contact, many liquid-solid couples undergo LME; a classic example is the embrittlement of aluminum alloys by liquid gallium.[10] While there is not a single, unified definition of LME, it is typically defined as the reduction in strength and/or ductility of a solid metal in contact with a liquid metal.[11] This umbrella description encompasses a number of different phenomenologies, including intergranular fracture (e.g., Al-Ga, Cu-Bi[12]), transgranular fracture (e.g., Al-Hg[13], Ni-Hg[14]), and liquid metal corrosion (e.g., W-Pu,[15] Fe-(PbBi eutectic)[16]). Within each of these phenomenologies, there are often apparent sub-mechanisms, including dependence on the oxygen concentration in the liquid.

The Ga-based liquid systems are of greatest importance for developing communications and electronic technologies due to their low melting point and non-toxic nature.[17,18] Eutectic Ga-In (eGaIn) is particularly attractive, as it is a liquid at room temperature. Ga-based liquids penetrate the grain boundary network of some solid metals, resulting in a rapid and catastrophic reduction in mechanical properties. While this sort of failure is widely reported, it also can result in a less-studied phenomenon: liquid-metal-mediated recrystallization (LMRX).

While LMRX has not been systematically studied, it has been observed in previous work. Electron backscatter diffraction (EBSD) mapping of tin-silver-copper exposed to liquid gallium illustrated rapid refinement of the solid grain structure, suggesting recrystallization occurred.[19] While the authors noted the grain refinement, recrystallization was not discussed. The early stages of recrystallization have been observed in ultra-fine-grained aluminum exposed to gallium, though only in the form of a few nano-scale new grains.[20] Tin single crystals decomposed into polycrystals as observed by Laue diffraction in specimens in which the gallium was applied with mechanical scratching, but not in specimens for which mechanical deformation was avoided.[21] Despite the first apparent report of the phenomenon being over 50 years ago, there has never been a systematic study of LMRX.

The objective of this work is to explore the dependence of LMRX on the initial structure of the solid metal. The Zn-eGaIn system was selected as an archetype of the intergranular mechanism because of the ease of handling and high contrast under backscattered imaging. This system is catastrophically embrittled within minutes of liquid

(Published online December 20, 2019)

exposure, but the microstructure continues to evolve over longer time scales. The liquid/solid metal interaction is measured as a function of initial solid grain size and extent of prior deformation in the solid.

EXPERIMENTAL METHODOLOGY

Commercially pure zinc sheet was exposed to eGaIn (nominally 21.4 wt% In, balance Ga) purchased from The Indium Corporation.

The Zn specimens were prepared to different initial conditions. First, fine- and coarse-grained microstructures were obtained by heat treatment in a fluidized sand bath. The fine initial microstructure was obtained by heat treating the as-received Zn sheet at 150°C for 10 s. The coarse-grained initial structure was obtained by heat treatment at 281°C for 24 h. The coarse- and fine-grained microstructures prior to rolling are shown in Fig. 1. These initial microstructures were rolled at room temperature to reductions in thickness up to 50%.

Specimens were prepared for exposure to eGaIn via mechanical polishing. Progressive grinding was performed with a final step of 1200 grit with silicon carbide paper. This was followed by a polishing step with 1-micron diamond in a glycol-based non-aqueous suspension. Specimens were sonicated in methanol to remove polishing media and oily residue between each step and before exposure to eGaIn. Microhardness indents were used as fiducial markers for subsequent imaging.

Prior to liquid exposure, EBSD of the initial structure was conducted on a region of each specimen approximately 600 μm by 450 μm in size. EBSD data were collected in an FEI Verios scanning electron microscope (SEM) using an Oxford Symmetry EBSD camera.

Liquid eGaIn was applied to the sheet normal and allowed to propagate along the sheet rolling direction for all specimens under no external load. Immediately after application of the liquid, the specimen was placed in a JEOL JSM-6010la SEM. BSE images were collected in timed intervals based on the rate of liquid penetration, allowing penetration rates to be measured. After full penetration of the liquid into the grain boundary network, a second EBSD scan is collected for the same regions of each specimen. After liquid exposure, careful handling was required to prevent the specimens from fragmenting under their own weight.

All EBSD data in this study were processed using the MTEX toolbox for MATLAB.[22]

Thermodynamic data for the zinc-gallium-indium system was calculated using Thermo-Calc software and the TCSLD3 Solder alloys V3.2 Database.[23]

RESULTS AND DISCUSSION

A sample time series is shown in Fig. 2 for the coarse-grained specimen rolled 45%. The liquid eGaIn appears in bright contrast in BSE imaging because of the high atomic number of In. As shown, the liquid initially appears at select locations along the grain boundary network before eventually forming a continuous layer visible at the mesoscale. At longer times, large bright contrast regions form. EBSD and electron dispersive spectroscopy (EDS) analysis indicated that these are grains of solid crystalline In. Animated GIFs of each of the discussed conditions are included in figures S1–S4 of the online supplementary material.

Unfortunately, the ternary phase equilibria of the Zn-Ga-In system have not been experimentally explored near room temperature. Some thermodynamic properties were measured for the ternary system at 470°C, but this does not offer tremendous insight into the phase behavior.[24] Both In and Ga binary systems with Zn are eutectic, both with eutectic compositions of approximately 4 at%. Further experimental study of the ternary phase equilibria is required to explain the observed phase evolution.

CALPHAD predictions of the system using the Thermoc-Calc TCSLD3 Solder Alloys v3.2 database[23] show that both Ga and In have relatively low solubilities in solid Zn: 0.47 and 0.0083 atomic

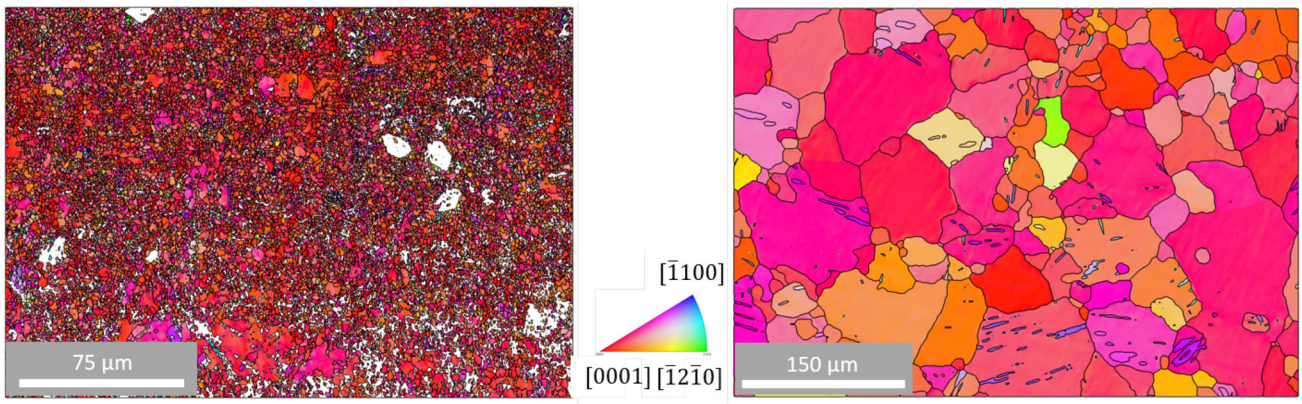

Fig. 1. Initial conditions for the fine- and coarse-grained microstructures.

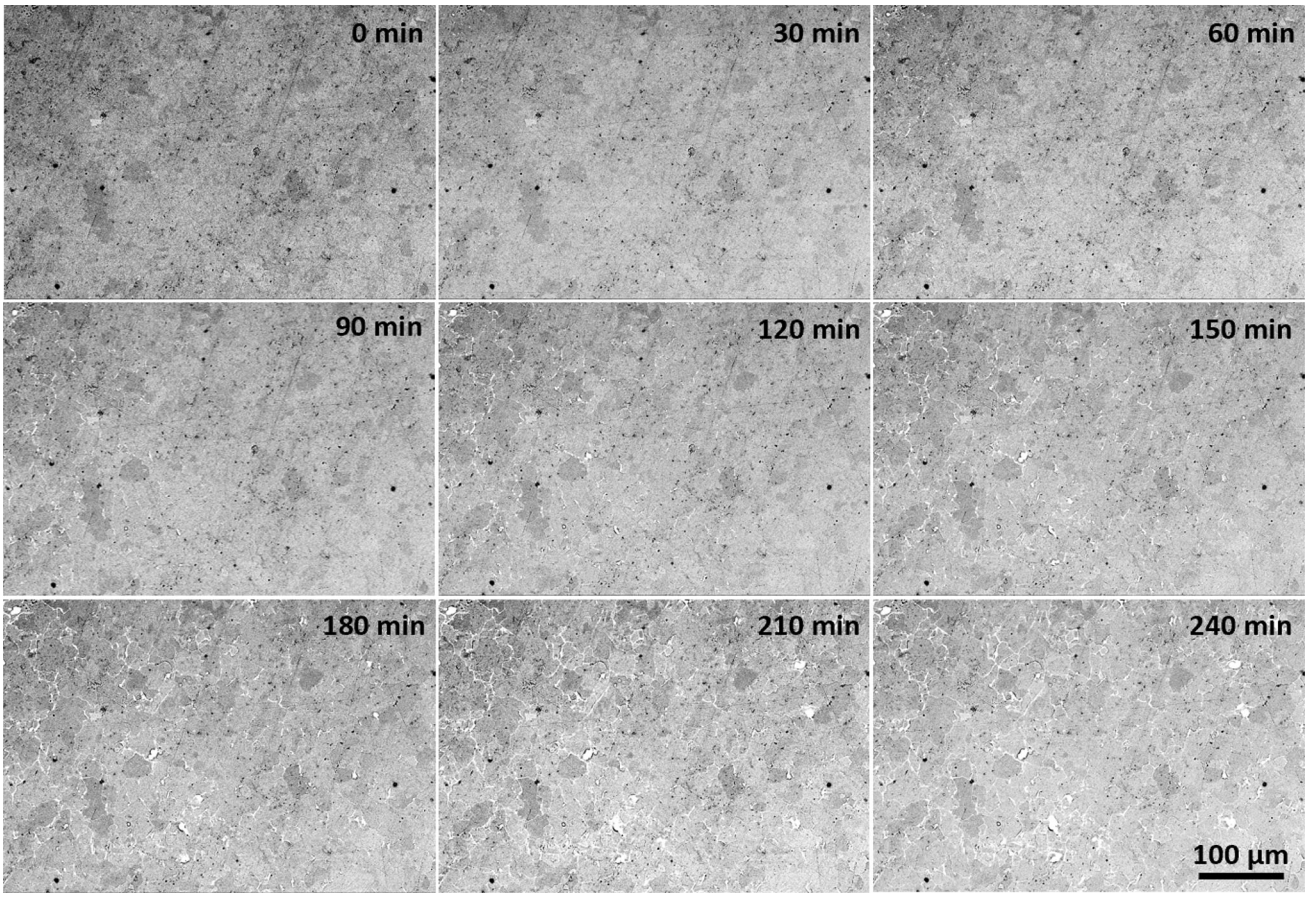

Fig. 2. Penetration of the liquid eGaIn into the Zn grain boundary network for the coarse-grained specimen rolled to a 45% reduction in thickness over 4 h at room temperature. Liquid propagation is from left to right in each frame.

percent, respectively, at 300K. The solubility of Zn in gallium-indium liquid alloys varies with indium concentration, ranging from 4.5% at very low indium concentrations to 2.9% at the gallium-indium eutectic. This suggests that the observed indium precipitation that occurs during propagation is likely due to an increased concentration of zinc in the liquid phase. Dissolution of the zinc is certainly occurring in parallel to the wetting process and may aid it by preferentially dissolving grain boundaries. Studies in other grain boundary wetting systems[25] suggest that dissolution can result in the widening of wetted grain boundaries to produce micron-scale films, much like those observed in the present study.

The distance covered by the liquid front as a function of time for a variety of initial grain sizes and roll reductions is presented in Fig. 3. The error bars represent the standard deviation of the measured distance traveled for five parallel segments of the same specimen. Linear fits are also included, and the average front velocities are shown on the plot. Variation in the rolling reduction had a minimal effect on the measured propagation rate, while variation in grain size altered the propagation rate by an order of magnitude.

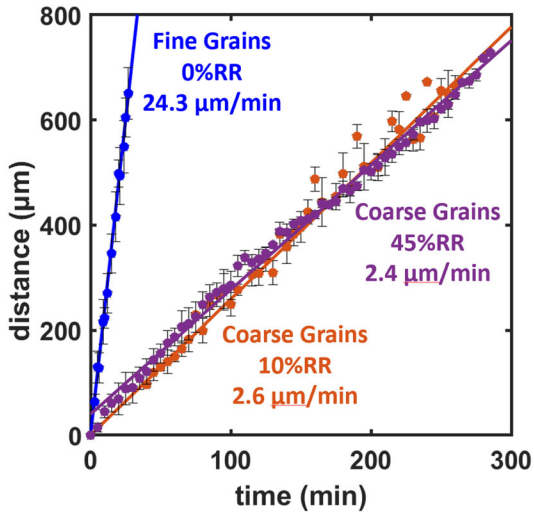

Fig. 3. Distance covered by the liquid front as a function of time for varied initial grain sizes and rolling reductions (RRs).

For some specimens, diffusion velocities were also measured along the Zn sheet transverse direction. Notably, no substantial variation in velocity was observed. This suggests that crystallographic

texture plays a relatively small role in diffusion velocity, at least when averaged over the complete grain boundary network.

EBSD was used to visualize the crystallographic changes to the microstructure before and after liquid metal exposure; an example microstructure (coarse-grained, 25% reduction in thickness) is shown in Fig. 4. Prior to liquid metal exposure, the grains contain strong orientation gradients, indicting a substantial stored dislocation density due to prior deformation. This is further demonstrated by the grain orientation spread (GOS) maps, where grains have GOS values up to 10°. Typically, GOS values < 1° indicate material that is recrystallized.[26,27] The grains are also nominally exquiaxed with some deformation twinning.

After exposure to the liquid, substantially more area is unindexable (white in maps). This typically corresponds to regions that were fine-grained prior to liquid exposure. The majority of the indexed grains do not correlate to any grain that existed in the initial structure; they are newly recrystallized.

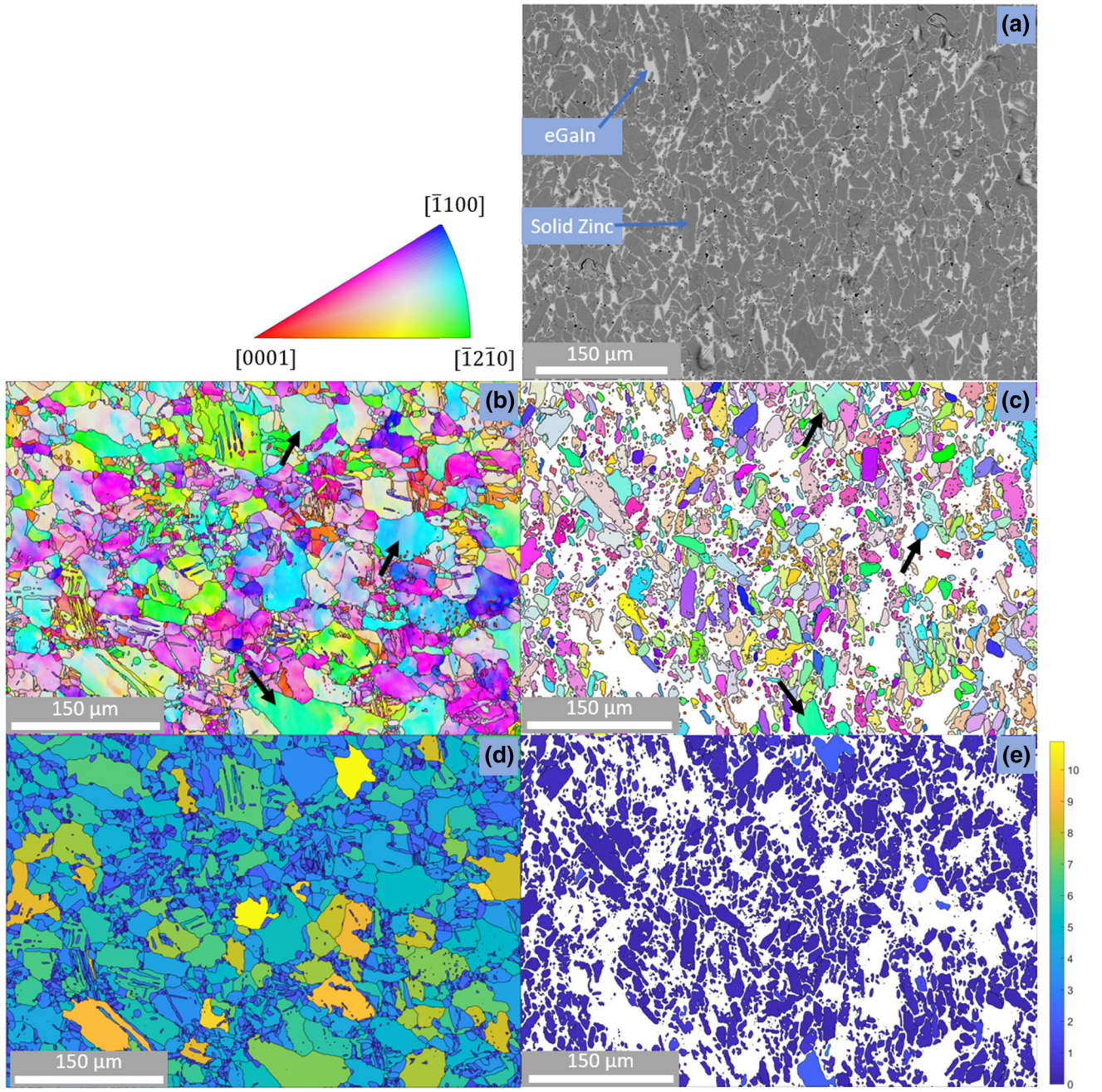

Fig. 4. BSE image of the microstructure after eGaIn infiltration (a). EBSD of Zn before (b, d) and after (c, e) exposure to eGaIn of a coarse-grained specimen rolled to a 25% reduction in thickness. In the middle row (b, c), inverse pole figure color is referenced to the normal direction. The last row (d, e) of images has grains colored by grain orientation spread.

Further evidence of recrystallization exists in the GOS maps, where nearly all grains have negligible internal misorientation after liquid exposure. However, some portions of the large grains remain. These are indicated with arrows and are particularly apparent in the post-liquid GOS map.

The post-exposure BSE map illustrates complete grain boundary wetting at all boundaries, but variable layer thickness. It also illustrates that some of the unindexed regions do still contain solid grains.

While the rolling reduction had negligible impact on the propagation rate of the liquid through the grain boundary network, it has a strong impact on the extent of recrystallization observed. This is illustrated in Fig. 5. In comparison to Fig. 4, substantially less recrystallization has occurred. This is consistent with traditional recrystallization behavior; specimens with a smaller rolling reduction have less stored energy and therefore a lower driving force for recrystallization. This suggests that the presence of the liquid is providing an easy kinetic pathway for recrystallization, potentially just by allowing for more rapid mass transport.

The recrystallized grains in the post-exposure microstructures have an apparent morphologic texture. While recrystallized grains would typically be equiaxed, these recrystallized grains are strongly elongated. Using MTEX, each grain was approximated as an ellipse, and the in-plane orientation was calculated. The projection of the crystallographic c-axis in the scan plane was also calculated.

The angle between the c-axis projection, $\vec{c}^{xy}_{crystal}$, and the minor axis of the fit ellipse, $\vec{b}^{xy}_{ellipse}$, was calculated for each grain, and histograms are plotted before and after liquid exposure in Fig. 6. In the initial structure, the morphologic and crystallographic textures are uncorrelated; there is no strong peak in the histogram. However, a strong correlation develops after exposure to eGaIn. The c-axis of each grain tends to align with the minor axis of the ellipse, at least as measured in the x-y plane.

While three-dimensional characterization would be necessary to definitively prove the relationship, this two-dimensional characterization suggests that exposure of Zn to eGaIn results in flat basal plates of Zn. Further support of this assertion is provided by the structure resulting from complete absorption of the liquid eGaIn by bulk Zn, illustrated in Fig. 7. Discoid single crystals of Zn nucleated and grew in the liquid droplet and then remained on the specimen surface after the liquid was fully absorbed by the substrate. A GIF of these crystals growing is shown in figure S-5 of the online supplementary material. These were confirmed to be single crystalline basal plates using EBSD. Note that these crystals often appear to be rounded hexagonal

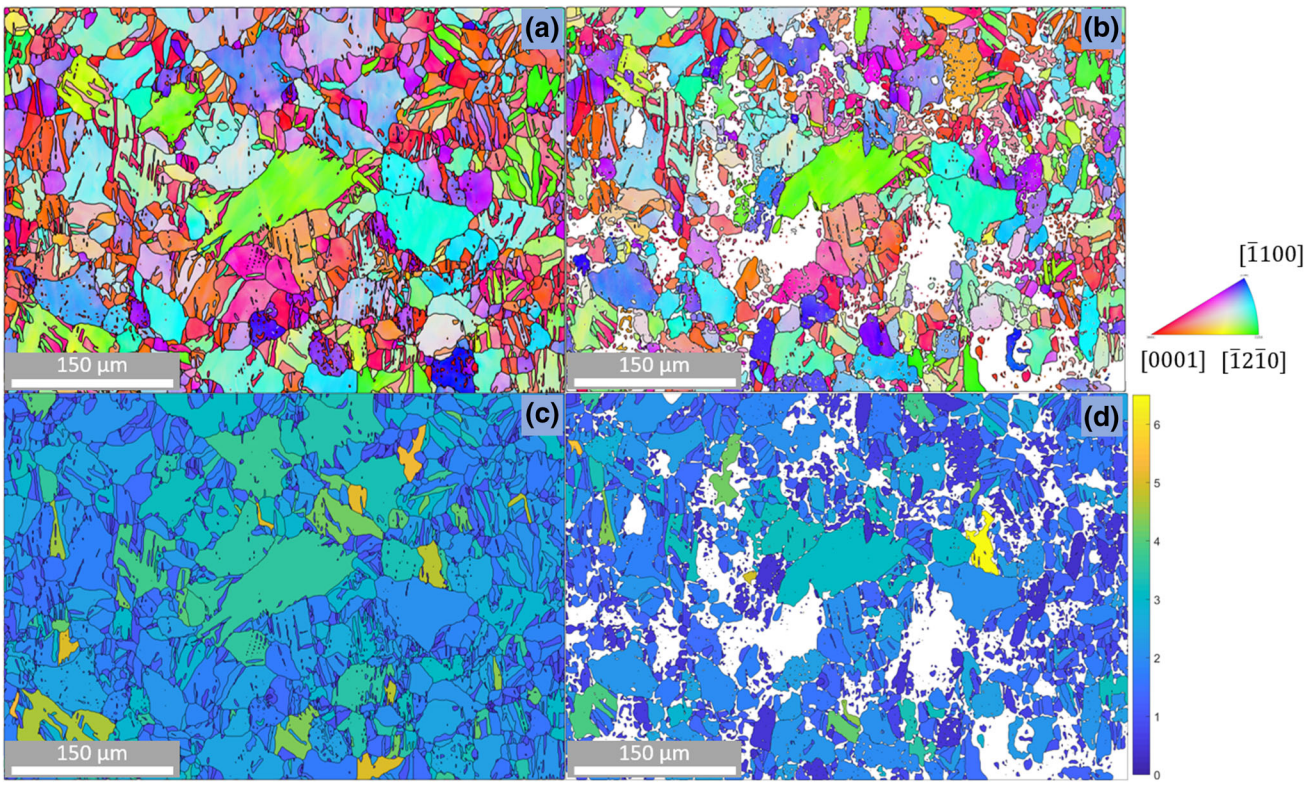

Fig. 5. Zn with at 10% RR before (a, c) and after (b, d) exposure to eGaIn. The top row (a, b) shows IPF maps colored with reference to the sheet normal, and the bottom row (c, d) are GOS maps.

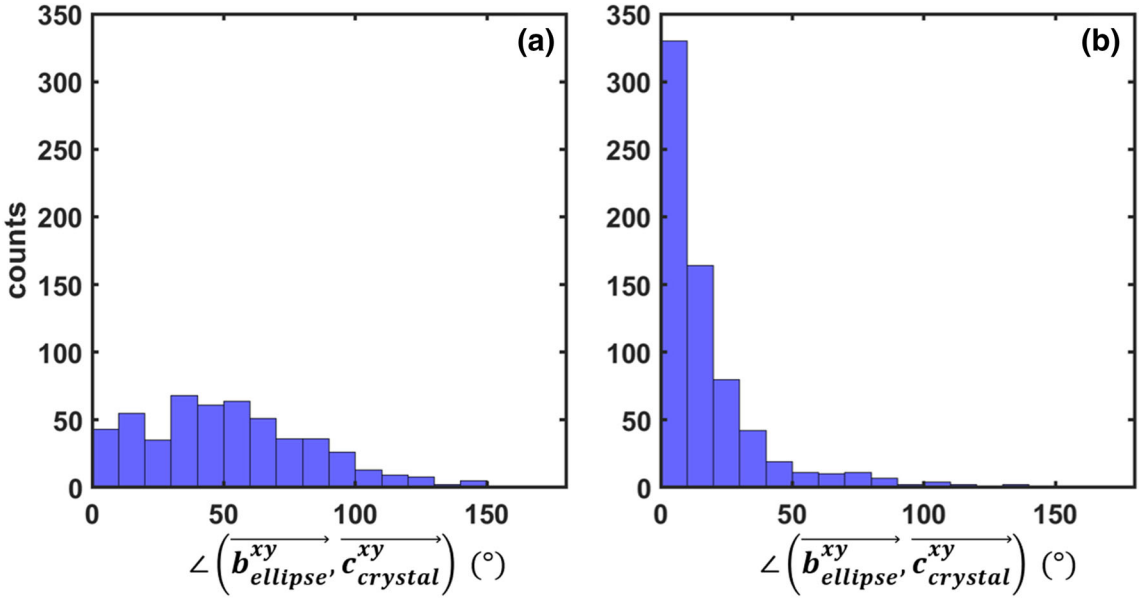

Fig. 6. Histograms of the angle between the *c*-axis projection and the minor axis of each Zn grain before (a) and after (b) eGaIn exposure for the coarse-grained 25% RR specimen.

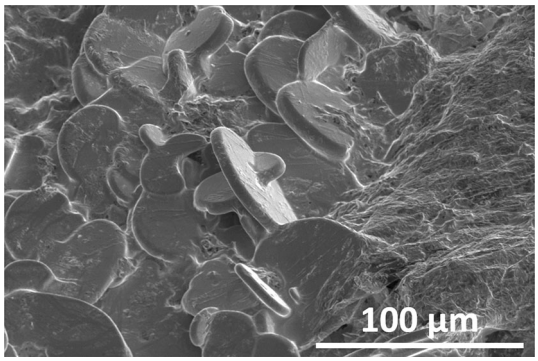

Fig. 7. Discoid single crystals of Zn that nucleated and grew in the liquid eGaIn and remained on the surface after the liquid was fully absorbed.

prisms. The aspect ratio of the discoids was compared with that of the recrystallized grains oriented to be "edge on" such that their crystallographic c-axis is perpendicular to the out of plane direction (tilted grains would appear thicker and skew the aspect ratio). The aspect ratio of recrystallized grains is on average much lower than that of the discoids, i.e., the discoids are much larger in diameter relative to their thickness compared with the bulk. The majority of "edge on" grain aspect ratios are < 3, while the discoids have aspect ratios in the range of 3–10. This may be a result of significantly increased crowding in the bulk relative to the crystals that grow in the droplet.

While the mechanism which results in the formation of discoid crystals in the droplet is unclear, there are some possible driving forces for this behavior. First, due to the increased chemical potential of the deformed surface, there will be a local increase in the solubility of zinc in the gallium-indium alloy near the interface. As this excess Zn diffuses further into the liquid, the melt would become supersaturated in zinc away from the interface. This supersaturation would provide a driving force for precipitation of the zinc crystals elsewhere in the melt. For this mechanism, it is of note that gallium oxide, present on the surface of the eGaIn droplet, could serve as a suitable nucleant for zinc crystal growth.[28] This mechanism is similar to the dissolution-condensation mechanism proposed for certain other types of liquid metal embrittlement systems, though Ga-Zn is not among them.[29] Another possible driving force is the enrichment of indium in the droplet following gallium penetration of the grain boundaries. As previously discussed, increased indium concentration in the melt lowers the solubility of zinc. However, this potential mechanism is less plausible because of the occurrence of solid indium precipitation throughout the percolated grain boundaries. The In precipitation indicates that indium is transported along with the gallium throughout the sample, suggesting that significant In enrichment of the liquid is unlikely.

More broadly, this series of experiments provides a framework allowing the characterization of the relative surface energies of solid-liquid interfaces and illustrates the importance of initial structure for contact stability in liquid circuit applications.

Moreover, the rapid evolution of a relationship between the morphologic and crystallographic texture could allow the engineering of solid contacts with greater stability in contact with liquid metals; if the solid grains are already in a highly stable orientation, they will tend to evolve less while in contact with a liquid. It has related design implications for the design of liquid metal-based slurries for

amalgam replacements. Amalgams and their Hg-free equivalents mix a liquid metal with a metallic powder to form a paste that fully solidifies. Hg-free "amalgams" are of interest for dental applications,[30–32] low-contact resistance electrodes,[33] solders,[34] interconnects,[35,36] and room-temperature metal additive manufacturing.[37] The evolution of grain morphology over time is likely to affect rheology and cure rate; tuning the shape of the solid particles based on interface stability could allow greater control over time-dependent flow behavior.

More fundamentally, consideration of liquid metal recrystallization offers a new interpretation of the intergranular liquid metal embrittlement mechanisms. The reported effects of prior strain on the severity of LME vary substantially from system to system. It is often the case that behavior is nonlinear even within a single system as a function of a third variable, most notably grain size.[38] The occurrence or absence of LMRX could offer a potential explanation for these seemingly contradictory results. Rapid near-surface recrystallization could also substantially alter the initial stages of fracture. Overall, LMRX has been under-considered in the discussion of LME. This study is far from comprehensive, but it reveals greater detail of the phenomenology of LMRX and illustrates that further study is warranted.

SUMMARY AND CONCLUSION

In summary, the present study explored the interaction between liquid eutectic gallium indium and solid zinc. It was demonstrated that the propagation rate of the liquid through the grain boundary network depends strongly on grain size, but has little dependence on prior deformation. However, the extent of recrystallization during exposure to the liquid metal depends strongly on the prior deformation.

During liquid-metal-mediated recrystallization, the recrystallized grains have an elongated morphology instead of the equiaxed morphology typical of most recrystallization mechanisms. The observed morphologies are consistent with basal plates, suggesting that the developed grain shapes are the result of surface energy minimization in contact with the liquid.

ACKNOWLEDGEMENTS

The authors thank M.D. Dickey for highly productive discussions throughout this project. This work is partially supported by the National Science Foundation award no. DMR-1842650. This work was performed in part at the Analytical Instrumentation Facility (AIF) at North Carolina State University, which is supported by the State of North Carolina and the National Science Foundation (award no. ECCS-1542015). The AIF is a member of the North Carolina Research Triangle Nanotechnology Network (RTNN), a site in the National Nanotechnology Coordinated Infrastructure (NNCI).

ELECTRONIC SUPPLEMENTARY MATERIAL

The online version of this article (https://doi.org/10.1007/s11837-019-03954-2) contains supplementary material, which is available to authorized users.

REFERENCES

1. F. Suarez, D.P. Parekh, C. Ladd, D. Vashaee, M.D. Dickey, and M.C. Öztürk, *Appl. Energy* 202, 736 (2017).
2. D.P. Parekh, C. Ladd, L. Panich, K. Moussa, and M.D. Dickey, *Lab Chip* 16, 1812 (2016).
3. M. Rashed Khan, G.J. Hayes, J.H. So, G. Lazzi, and M.D. Dickey, *Appl. Phys. Lett.* 99, 013501 (2011).
4. G.J. Hayes, J.H. So, A. Qusba, M.D. Dickey, and G. Lazzi, *IEEE Trans. Antennas Propag.* 60, 2151 (2012).
5. A. Qusba, A.K. RamRakhyani, J.H. So, G.J. Hayes, M.D. Dickey, and G. Lazzi, *IEEE Sens. J.* 14, 1074 (2014).
6. K. Khoshmanesh, S.Y. Tang, J.Y. Zhu, S. Schaefer, A. Mitchell, K. Kalantar-zadeh, and M.D. Dickey, *Lab Chip* **17**, 974 (2017).
7. I.D. Joshipura, H.R. Ayers, C. Majidi, and M.D. Dickey, *J. Mater. Chem. C* 3, 3834 (2015).
8. S. Zhu, J.H. So, R. Mays, S. Desai, W.R. Barnes, B. Pourdeyhimi, and M.D. Dickey, *Adv. Funct. Mater.* 23, 2308 (2013).
9. M.G. Mohammed and M.D. Dickey, *Sens. Actuators A Phys.* Complete, 246 (2013).
10. W. Rostoker, *Embrittlement by Liquid Metals* (Reinhold Publishing Corporation, New York, 1960).
11. M.H. Kamdar, *Embrittlement of Engineering Alloys, Volume 25 of Treatise on Materials Science and Technology* (Academic Press Inc., New York, 1983).
12. N.V. Pertsov and P.A. Rebinder, *Dokl. Akad. Nauk SSSR* 123, 1068 (1958).
13. F.N. Rhines, J.A. Alexander, and W.F. Barclay, *Trans. ASM* 55, 22 (1962).
14. S.P. Lynch, *Scr. Metall.* 13, 1051 (1979).
15. D.R. Lesuer, J.B. Bergin, S.A. McInturff, and B.A. Kuhn, *Microstruct. Sci.* 9, 256 (1981).
16. D. Sapundjiev, S. Van Dyck, and W. Bogaerts, *Corros. Sci.* 48, 577 (2006).
17. Y. Lu, Q. Hu, Y. Lin, D.B. Pacardo, C. Wang, W. Sun, F.S. Ligler, M.D. Dickey, and Z. Gu, *Nat. Commun.* 6, 10066 (2015).
18. M.D. Dickey, *Adv. Mater.* 29, 1606425 (2017).
19. E. Nguena, D. Danovitch, M. Kanso, and R. Langlois, *IEEE* (2017), pp. 1584–1591.
20. M. Naderi, M. Peterlechner, E. Schafler, S.V. Divinski, and G. Wilde, *Acta Mater.* 99, 196 (2015).
21. V.I. Likhtman, E.D. Shchukin, and P.A. Rebinder, *Physicochemical Mechanics of Materials*, Chap. 5. (Israel Program for Scientific Translations, Jerusalem, Israel, 1962).
22. F. Bachmann, R. Hielscher, and H. Schaeben, *Solid State Phenom.* 160, 63 (2010).
23. Thermo-Calc, TCSLD3 Solder Alloys database (2019).
24. W.J. Svirbely and S.M. Read, *J. Phys. Chem.* 66, 658 (1962).
25. K. Wolski and V. Laporte, *Mater. Sci. Eng. A* 495, 138 (2008).

26. L.N. Brewer, D.P. Field, and C.C. Merriman, *Electron Backscatter Diffraction in Materials Science* (Springer, Boston, MA, 2009), pp. 251–262.
27. V.M. Miller, Texture evolution during thermomechanical processing in rare earth free magnesium alloys. PhD dissertation, University of California Santa Barbara, Santa Barbara, CA (2016).
28. A. Jain, S.P. Ong, G. Hautier, W. Chen, W.D. Richards, S. Dacek, S. Cholia, D. Gunter, D. Skinner, G. Ceder, and K.A. Persson, *APL Mater.* 1, 011002 (2013).
29. E.E. Glickman, *Defect Diffus. Forum* 264, 141 (2007).
30. H. Herø, C.J. Simensen, and R.B. Jørgensen, *Biomaterials* 17, 1321 (1996).
31. M.R. Pinasco, E. Angelini, E. Cordano, and F. Rosalbino, *J. Alloy. Compd.* 317–318, 411 (2001).
32. D.L. Smith and H.J. Caul, *J. Am. Dent. Assoc.* 53, 315 (1956).
33. G.G. Harman, *Rev. Sci. Instrum.* 31, 717 (1960).
34. S. Sommadossi, H.E. Troiani, and A. Fernández Guillermet, *J. Mater. Sci.* 42, 9707 (2007).
35. D.F. Baldwin, R.D. Deshmukh, and C.S. Hau, 1996 Proceedings 46th Electronic Components and Technology Conference (1996), pp. 1143–1150.
36. C.A. MacKay, *IEEE Micro* 13, 46 (1993).
37. M.D. Dickey, Liquid-Solid Mixtures for Additive Patterning of Solid Metals at Room Temperature (unpublished) (2019).
38. R. Rosenberg and I. Cadoff, in *Fracture of Solids*, ed. by D.C. Drucker, J.J. Gilman (Interscience, New York, 1963), p. 607.